Asymmetric spatial power beam splitter based on all dielectric metasurface with transmission phase

JIANMIN LI[1], PENG CHEN[2], BO FANG[2,*], JINHUI CAI[2], LE ZHANG[2], JIANXUN LU[3], YINGLAI WU[4], WENKANG HUANG[5], LIBO XU[6], CHENXIA LI[6], XUFENG JING[6]
[1]*University of Shanghai for Science and Technology, No. 516 Jung Gong Road, Shanghai 200093, China*
[2]*College of Metrology & Measurement Engineering, China Jiliang University, Hangzhou 310018, China*
[3]*Zhejiang Smart Information Technology, Co., Ltd., Jinhua, 321000, PR China*
[4]*School of entrepreneurship, Hangzhou Dianzi University, Hangzhou 310000, China*
[5]*Zhejiang Institute of Economics & Trade, Hangzhou 310018, China*
[6]*Institute of Optoelectronic Technology, China Jiliang University, Hangzhou 310018, China*

In order to freely manipulate electromagnetic beam, a transmissively coded metasurface beam splitter is proposed. The unit structure of the coded metasurface can be constructed by using polyimide as substrate and quadrate silicon column as dielectric scattering resonance cell. By changing the height of the square column of silicon material, the transfer phase of the cell structure can be changed. These unit structures with certain phase difference and large transmission amplitude can be encoded to construct the all dielectric coded metasurface. Based on different coding arrangement, different angles and different numbers of beam splitting can be achieved. By changing the incident angle, multiple beams with different energy distribution ratio can be obtained. Asymmetric spatial power beam splitter can be realized by using these encoding metasurfaces. Based on the phase array antenna principle, the calculated scattering angle agrees well with that of the numerical simulation.

(Received August 18, 2021; accepted June 6, 2022)

Keywords: Metasurface, Metamaterials, Optics devices, Terahertz

1. Introduction

Metamaterial refers to a composite material with an artificially designed structure that does not exist in nature but exhibits extraordinary physical properties not found in natural materials. Because of their special structure, metamaterials can achieve effects that natural materials cannot, such as allowing light and electromagnetic waves to change their usual properties [1-10]. Due to the complexity of the experimental preparation of metamaterials and the problem of the overall loss of materials, researchers have recently focused on the study of metamaterials' two-dimensional counterparts, namely metasurface [11-20]. Metasurface is an artificial electromagnetic surface composed of array of subwavelength scatterers. It has super electromagnetic wave processing ability, and can realize accurate and effective control of electromagnetic wave propagation mode, amplitude, polarization, phase and other characteristics [21-30]. Because of its ultra-thin thickness, the metasurface take up much less physical space and have less material loss. Therefore, metasurface may lead to many applications, such as ultra-sensitive sensors, polarization converters, focusing lenses, cloaking, holographic imaging, etc. [31-35].

In recent years, with the development of micro-machining and nanotechnology, ultra-thin optical device technology has developed rapidly. More and more optical components are integrated into a single chip for large-scale photonic integrated circuit optics. However, many traditional optical devices, such as lenses and wave plates, are designed using volume materials, which are relatively large in size, making it difficult to achieve optical integration and miniaturization. However, optical devices based on metasurfaces, due to their advantages such as small size, convenient tuning, controllable electromagnetic wave and integration, are gradually replacing traditional optical devices and developing rapidly as a new and hot technology [36-38].

The beam splitter is an essential component in photoelectric system, which can split one beam into two or more beams, and is the key part of most interferometers. Power beam splitters are usually made of metal or dielectric films, and the beam splitters are still made of bulk materials. As technology improves, optical devices need to be made smaller and smaller, which requires metasurface technology. In this work, we design a transmissive space power beam splitter in the terahertz band based on the all dielectric transmission phase metasurface with step height variation. We can change the

transmission phase by changing the thickness of the square cylindrical element structure. We encode the unit structures of different phase response, construct different encoding sequence metasurface, and realize the design of two-beam, four-beam and multi-beam splitter.

2. Far field scattering of encoding metasurface

The far-field energy scattering characteristics of a terahertz beam splitter are mainly determined by the structural arrangement characteristics of the coded metasurface elements. In order to clearly understand the physical mechanism of the scattering energy beam splitter, we introduce the traditional phased array antenna theory. The traditional phased array antenna theory can be used to explain the scattering principle of coded metasurface. Coding metasurface refers to assigning numeric codes to each element of a metasurface structure. For 1-bit coded metasurface, it means that the metasurface is composed of two kinds of unit structures, the phase difference of the two kinds of unit structures just satisfies π, and the two kinds of units are denoted by "0" and "1". For 2-bit coding, the metasurface means that the metasurface is made up of four units with phase differences π/2. These four units are represented by "00", "01", "10" and "11", respectively.

Firstly, we assume that there are two encoding unit structures and encode them as "0" and "1" respectively. d_x *and* d_y indicate the length of each encoding unit in *x*-direction and *y*-direction, respectively. Using these two coding particles, we constructed a checkerboard coding metasurface as "10101010…/01010101…". The coded metasurface consists of M* N unit structures, where M represents the number of unit structures in the *x* direction and N represents the number of unit structures in the *y* direction. The reflection or transmission phase in encoding unit is set to be ϕ (m,n), where (m, n) indicates the corresponding position of a coding unit on the coding metasurface. When a plane electromagnetic wave hits the coded metasurface at a normal incidence, the far-field scattering of the metasurface can be expressed as [39,40]

$$\mathrm{F}(\theta,\varphi)=\sum_{m=1}^{M}\sum_{n=1}^{N}T_{m,n}e^{-i\left(kd_x\left(m-\frac{1}{2}\right)\sin\theta\cos\varphi+kd_y\left(n-\frac{1}{2}\right)\sin\theta\sin\varphi\right)}, \tag{1}$$

where $T_{m,n}$ shows the transmitted coefficient for encoding unit, *k* is wave vector, and θ and φ are elevation and azimuth angles of scattering. It is assumed that the transmission coefficient of each coding unit is 1, and the phase of each coding unit is 0 or π. Equation (1) can be simplified as

$$\mathrm{F}(\theta,\varphi)=\sum_{m=1}^{M}e^{-i\left(kd_x\left(m-\frac{1}{2}\right)\sin\theta\cos\varphi+m\pi\right)}\sum_{n=1}^{N}e^{-i\left(kd_y\left(n-\frac{1}{2}\right)\sin\theta\sin\varphi+n\pi\right)} \tag{2}$$

We can further obtain as

$$|F(\theta,\varphi)|=MNSinc\left(m\pi\left(p+\frac{1}{2}\right)-\frac{m}{2}kd_x\sin\theta\cos\varphi\right)Sinc\left(n\pi\left(q+\frac{1}{2}\right)-\frac{n}{2}kd_y\sin\theta\sin\varphi\right), \tag{3}$$

where p, q=0, ±1, ±2.... It can be deduced from Eq. (3) that $|\mathrm{F}(\theta,\varphi)|$ reaches its first extreme value, when it satisfy the following conditions as

$$\varphi=\pm tan^{-1}\frac{d_x}{d_y},\varphi=\pi\pm tan^{-1}\frac{d_x}{d_y}, \tag{4}$$

$$\theta=sin^{-1}\left(\frac{\pi}{k}\sqrt{\frac{1}{d_x^2}+\frac{1}{d_y^2}}\right). \tag{5}$$

When $\Gamma_x=2d_x$, $\Gamma_y=2d_y$, and $k=2\pi/\lambda$, Eq.(7) can be simplified as

$$\theta=sin^{-1}\left(\lambda\sqrt{\frac{1}{\Gamma_x^2}+\frac{1}{\Gamma_y^2}}\right). \tag{6}$$

Γ_x and Γ_y indicate the super period of encoding metasurface in *x*-direction and *y*-direction, respectively. If $\Gamma_x\to\infty$, or $\Gamma_y\to\infty$, Eq.(6) for the elevation angle θ of the anomalous beam can be simplified as

$$\theta=sin^{-1}\left(\frac{\lambda}{\Gamma}\right), \tag{7}$$

where Γ indicates coding period in the encoding direction.

3. Power beam splitter of all dielectric metasurface

In order to design a power splitter, we should first design the unit structure of the device. Fig. 1 shows the schematic diagram of the structure of an all-medium metasurface unit. We used polyimide as the base material and silicon as the dielectric material for scattering resonator. The unit structure period X is X = 150, and the base thickness is *d* = 20 μm. The side length of the square silicon column is *a* = 100 μm. The height *h* of the square column is a variable. By changing the height H of the square column, the required compensating phase can be

obtained. The step height change mentioned in this paper refers to the height change of the square column, which is used to control the phase change between the unit structures.

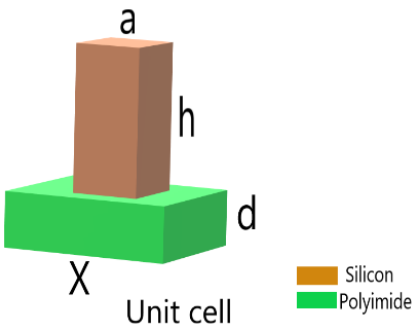

Fig. 1. Schematic diagram of the structure of an all-medium metasurface unit (color online)

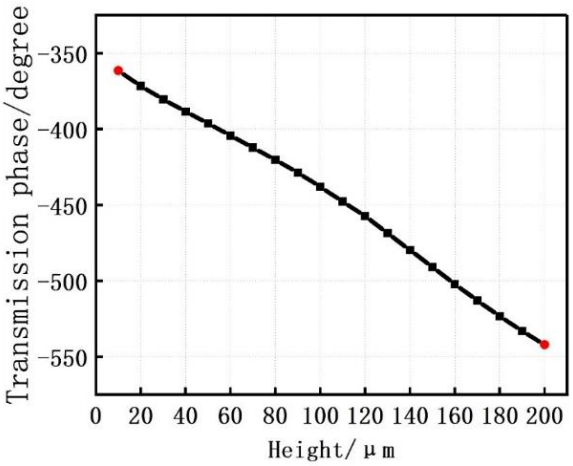

(a)

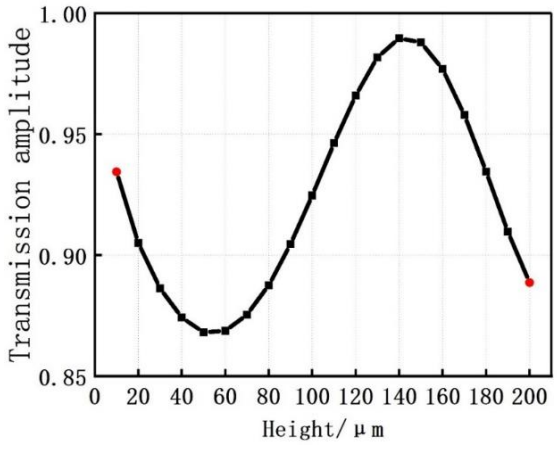

(b)

Fig. 2. (a)The relationship between the transmission phase response of periodic element structure and the height of square column, (b) The transmission amplitude response of periodic element structures as a function of the height of square columns

Using the finite integral method, we numerically calculated the transmission amplitude and phase of the periodic element structure. Fig. 2(a) shows the relationship between the transmission phase response of periodic element structure and the height of square column. The designed cell provides phase control by varying the height of the square column. As can be seen from the phase response curve in Fig. 2(a), when the height is 10 μm and 200 μm, the transmission phase under normal incidence is equal to -362° and -542°, respectively. The phase difference between the two cells is approximately equal to 180°. Therefore, the two cells can be used to construct 1-bit coded metasurface arrays to achieve the desired scattering patterns. Another important factor to consider is the transmission amplitude of the cell, which has a direct effect on the efficiency of the entire coded metasurface. Fig. 2(b) indicates the transmission coefficient response of periodic element structures as a function of the height of square columns. As shown in Fig. 2(c), at h = 10 μm and h = 200 μm the transmission amplitudes are all greater than 0.88. This means that the designed metasurface has high transmission efficiency. Based on π phase difference and high transmission amplitudes of the two kinds of element structures, we can select these two kinds of element structures to construct 1-bit coded metasurface and realize the splitting characteristics of energy beams.

To quantitatively exhibit the beam splitting of encoding metasurface, we can encode the 1-bit metasurface with the coding sequence of "10101010…" as shown in Fig. 3. It can be presented by repeating a corresponding coding matrix as $M_1^{1-bit} = \begin{bmatrix} 10101010\ldots \\ 10101010\ldots \end{bmatrix}$. Due to the coupling effect between adjacent coding particles, the energy splitting ability of electromagnetic wave will be weakened. To decrease this unwanted coupling effect, we used the super coding particles, which is composed of the elemental coding particles with size 4*4. Fig. 3 shows the corresponding far field scattering of two beams of energy splitting. The incideng wave direction is along +z direction. Because the metasurface unit structure is distributed gradually along the x-axis, the terahertz wave will be transmitted under the metasurface in the form of double beams when the terahertz wave is normally incident on the metasurface in the z-axis. The two scattered beams should be in the xoz plane. The two beams will be exactly symmetrical about the z-axis. According to the Eq.(7) as $\theta = \sin^{-1}\left(\frac{\lambda}{\Gamma}\right)$, the scattering angle can be calculated accurately. On the basis of $\lambda = 666$ μm and Γ = 8*150 μm = 1200 μm, the

scattering angle can be calculated as θ=33.71° . In the numerical simulation, the splitting angle of the beams is 32°. It can be seen that the result of theoretical calculation agrees with the result of numerical simulation.

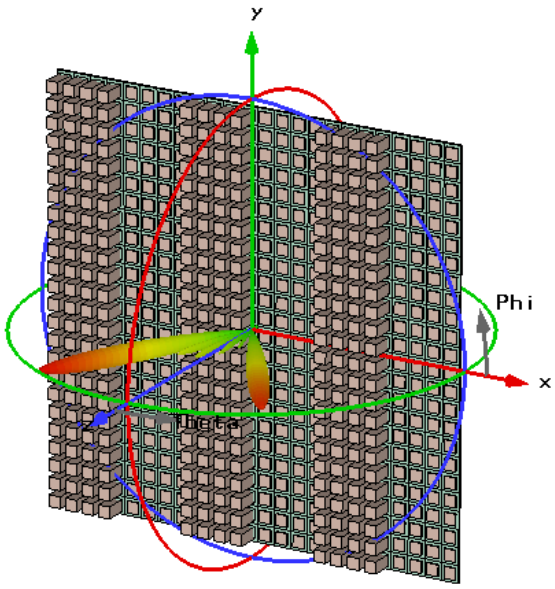

Fig. 3. 1-bit encoding metasurface with the coding sequence of "10101010…"and far-field scattering of two beams of energy splitting (color online)

Next, we construct the checkerboard coded metasurface to realize the four-beam splitting property. Fig. 4 shows the schematic diagram of the checkerboard coded metasurface. It can be presented by repeating a corresponding coding matrix as $M_2^{1-bit} = \begin{bmatrix} 10101010 \ldots \\ 01010101 \ldots \end{bmatrix}$. When a terahertz wave is normally incident on the checkerboard coded metasurface, four beams can be split, and each beam has roughly the same energy. From the scattered beam characteristics, we can know that different scattered beam characteristics can be obtained for different encoding modes. This may be based on the principle of interference of electromagnetic waves.

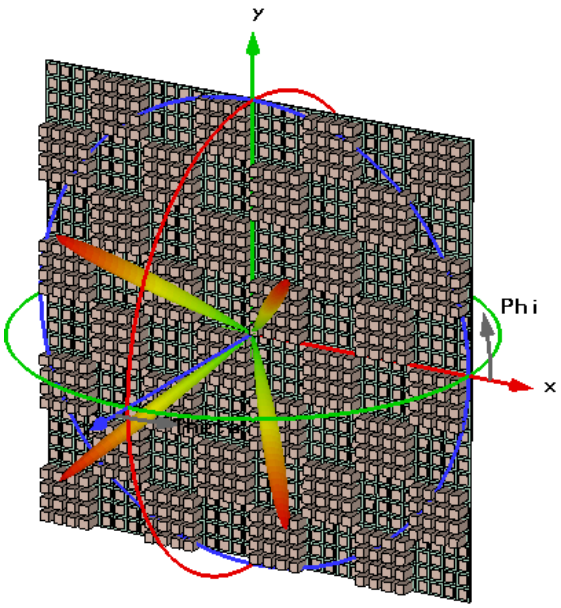

Fig. 4. Schematic diagram of the checkerboard coded metasurface, and far-field scattering of four-beam splitting (color online)

The simulation discussed above is the case of normal incident light, and we obtain symmetric beam splitting. In order to obtain asymmetric beam splitting properties, the oblique incidence of a terahertz wave can be applied. For the encoding metasurface sequence M_1, the far field scattering of beams is shown in Fig. 5(a) when a terahertz wave is incident with the incident angle of 5°. At this time, the double-beam splitter still scatters two beams of light, but the power distribution and scattering Angle of the beams are different, and the energy of one beam is significantly greater than that of the other beam. This phenomenon is different from the uniform energy distribution of the two beams under normal incidence. Therefore, we can adjust the incident angle appropriately to control the separation angle and power distribution of the scattered beam. When the incident angle is -10°, the scattered energy distribution is shown in Fig. 5(b). Obviously, the energy of the two splitting terahertz waves is different. Based on the far-field scattering characteristics, we can know that in addition to the main lobe scattering, there are other small side lobe scattering in the scattered beam. This may be related to the small number of particles we are counting. If we increase the number of computing elements, the sidelobes of far-field scattering may decrease or disappear. However, this may result in a larger amount of computation and longer computation time. When the incident angle is further increased, we can speculate that the scattered beam will be further tilted. At a certain angle, part of the scattered beam may disappear and the reflected light energy will gradually increase.

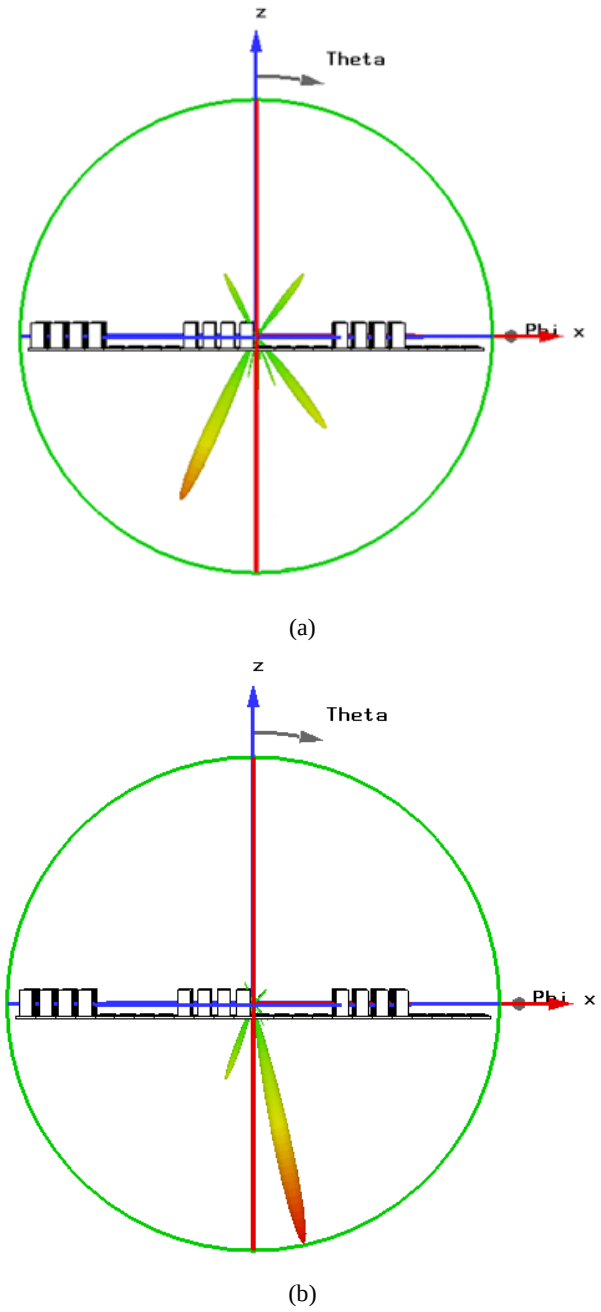

Fig. 5. Side view of far-field scattering for the encoding metasurface sequence "10101010…" when the terahertz wave is oblique. (a) Incident angle of 5°, (b) Incident angle of -10° (color online)

Similarly, we can adjust the energy distribution of the four beams on the checkerboard coded metasurface M_2. Fig. 6(a) shows the top view of far-field scattering for the encoding metasurface sequence "10101010…/01010101…" when the terahertz wave is incident with the angle of 5°. We know that the four beams scattered by the beam splitter at normal incidence have the same power, while two of the four beams scattered at oblique incidence have significantly greater energy than the other two. We can further adjust the energy distribution ratio of the four beams by changing the incident angle as shown in Fig. 6(b). This kind of beam splitter based on metasurface is more convenient and flexible to realize beam scattering at any angle and arbitrary power. The beam splitter based on metasurface is thinner than the traditional beam splitter, and more convenient to integrate the optical system.

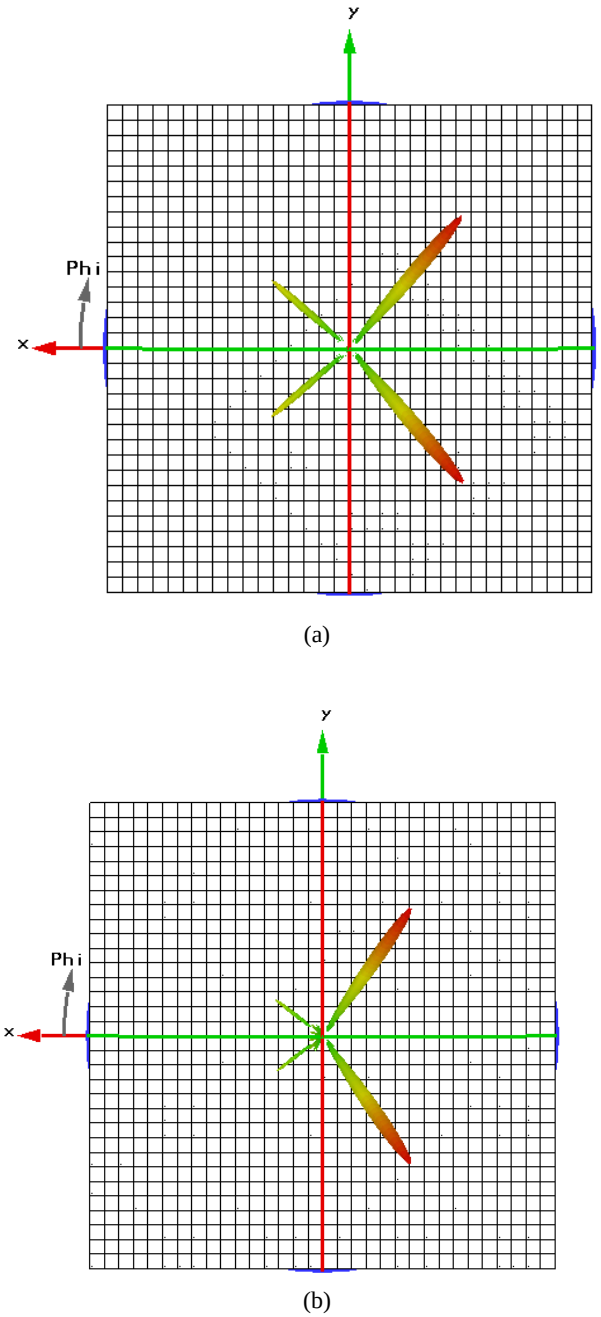

Fig. 6. Top view of far-field scattering for the encoding metasurface sequence "10101010…/01010101…" when the terahertz wave is oblique. (a) Incident angle of 5°, (b) Incident angle of 10° (color online)

The above designs are all 1-bit coded metasurface, and the designed metasurface structure is relatively simple. In order to achieve more complex and changeable spectral effects, multi-bit coding can be used to design more complex metasurface. After optimizing the design, we found that when h = 10 μm, h = 110 μm, h = 200 μm and h = 300 μm, the phase difference of the four-cell structure is 90°, and the transmission amplitudes of the four element structures are all greater than 0.88. Therefore, we can use these four cell structures to build 2-bit coded metasurface. These unit particles can be encoded as "0", "1", "2", and "3". Using the designed 2-bit four-cell structures, the coded metasurface is arranged into a gradual phase distribution with the sequence "01230123…" as shown in Fig. 7. It can be presented by repeating a corresponding coding matrix as $M_3^{2-bit} = \begin{bmatrix} 01230123\ldots \\ 01230123\ldots \end{bmatrix}$. The corresponding far-field scattering is shown in Fig. 7. We can find that there is only one deflected beam for the phase-gradient encoded metasurface. Due to the limitation of the number of particles, the phenomenon of side lobe appears in the far-field scattering. It is worth noting that, based on the generalized Snell's law, we can change the number of repetitions of the coded particles to achieve different deflection angles.

In order to obtain the free control of scattering angle in three-dimensional space, the different coding arrangement should be applied. If the code particles are arranged along a diagonal line of the metasurface as a gradient phase distribution, we can get a scattered beam with an azimuth of 45°. Fig. 8 shows the schematic diagram of coded metasurface with diagonal phase gradient. The corresponding far field scattering is indicated in Fig. 8. From 1-bit coding to 2-bit coding, the degree of freedom of the arrangement of unit particles is increased. If one wants to obtain the beam distribution of different angles and different numbers, and the energy of the beam splitting is in a certain proportion in multiple directions, one can simply change the arrangement of coding particles and use different incident angles to achieve these functions. The coded metasurface beam splitter, which is not limited to the number and angle of the beam, can be used to control the terahertz wave flexibly. Asymmetric spatial power splitters with variable beam splitter angles and power distribution are needed in photonic integrated systems, and the encoded metasurface may be used in photonic integrated systems.

Even though the presented work is fully based on numerical simulations of encoding metasurfaces, it is feasible to prepare such all dielectric encoding metasurfaces. The longer wavelength of THz waves requires an alternate fabrication process which is different to that previously described in the visible and infrared spectrum [41]. Detailed preparation process of all dielectric metasurfaces in terahertz range refers to Ref. [41]. The preparation processes include the base bonding, the conventional mask photolithography, and the Bosch deep reactive ion etching process [42].

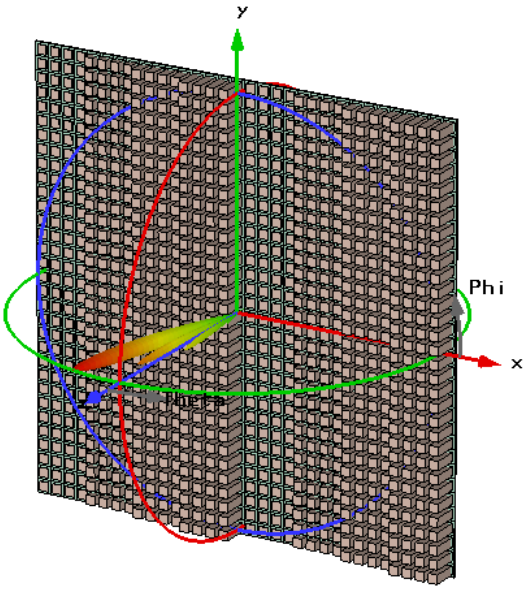

Fig. 7. Coded metasurface with gradient phase distribution with the encoding sequence "01230123…", and far field scattering of coded metasurface (color online)

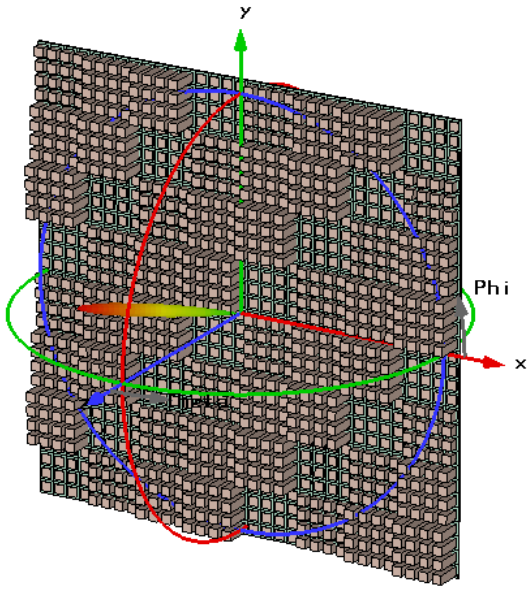

Fig. 8. Schematic diagram of coded metasurface with diagonal phase gradient, and the corresponding far-field scattered beam (color online)

4. Conclusions

In this paper, a novel beam splitter operating in the terahertz band is proposed. Compared with the traditional bulky optical devices, this metasurface based beam splitter can be applied to integrated optical systems. The beam splitter operates in the terahertz band and forms the gradual phase based on the step height change of unit cells. The number, angle and power distribution ratio of the separated beams can be controlled by the coded metasurface beam splitter through different coding distributions.

Acknowledgment

This work was supported by National Key R&D Program of China (No. 2018YFF01013005); Fundamental Research Funds for the Provincial Universities of Zhejiang (No. 2021YW09）;National Natural Science Foundation of China (No.62175224, No. 52076200); New-shoot Talents Program of Zhejiang province (No. 2021R409042); Natural Science Foundation of Zhejiang Province (No. LZ21A040003, No. LY20F050007, No. LY22F050001).

References

[1] Xiaoyong He, Feng Liu, Fangting Lin, Wangzhou Shi, J. Phys. D: Appl. Phys. **54**, 235103 (2021).
[2] Jun Peng, Xiaoyong He, Chenyuyi Shi, Jin Leng, Fangting Lin, Feng Liu, Hao Zhang, Wangzhou Shi, Physica E **124**, 114309 (2020).
[3] Xiaoyong He, Feng Liu, Fangting Lin, Wangzhou Shi, Opt. Lett. **46**, 472 (2021).
[4] X. He, X. Zhong, F. Lin, W. Shi, Opt. Mater. Express **6**, 331 (2016).
[5] Jinxing Li, Yueyi Yuan, Qun Wu, Shah Nawaz Burokur, Kuang Zhang, Chin. Opt. Lett. **19**, 100501 (2021).
[6] S. Teng, Q. Zhang, H. Wang, L. Liu, H. Lv, Photonics Research **7**(3), 246 (2019).
[7] M. R. Akram, G. Ding, K. Chen, Y. Feng, W. Zhu, Advanced Materials **32**, 1907308 (2020).
[8] J. Zhang, X. Wei, I. D. Rukhlenko, H.-T. Chen, W. Zhu, ACS Photonics **7**(1), 265 (2020).
[9] Haoyu Wang, Zhiyu Zhang, Kun Zhao, Wen Liu, Pei Wang, Yonghua Lu, Chin. Opt. Lett. **19**, 053601 (2021).
[10] Bo Fang, Zhiyu Cai, Yandong Peng, Chenxia Li, Zhi Hong, Xufeng Jing, Journal of Electromagnetic Waves and Applications **33**(11), 1375 (2019).
[11] B. Fang, B. Li, Y. Peng, C. Li, Z. Hong, X. Jing, Microw. Opt. Technol. Lett. **61**, 2385 (2019).
[12] Weimin Wang, Xufeng Jing, Jingyin Zhao,Yinyan Li,Ying Tian, Optica Applicata **47**(2), 183 (2017).
[13] L. Jiang, B. Fang, Z. Yan, C. Li, J. Fu, H. Gan, Z. Hong, X. Jing, Microwave and Optical Technology Letters **62**(6), 2405 (2020).
[14] Xinhua Xie, Yunpei Deng, Steven L. Johnson, High Power Laser Science and Engineering **9**(4), 04000e66 (2021).
[15] Yi Zhao, Qiuping Huang, Honglei Cai, Xiaoxia Lin, Hongchuan He, Hao Cheng, Tian Ma, Yalin Lu, Chin. Opt. Lett. **19**, 073602 (2021).
[16] Hafiz Saad Khaliq, Inki Kim, Aima Zahid, Joohoon Kim, Taejun Lee, Trevon Badloe, Yeseul Kim, Muhammad Zubair, Kashif Riaz, Muhammad Qasim Mehmood, Junsuk Rho, Photonics Research **9**(9), 09001667 (2021).
[17] Matthew Parry, Andrea Mazzanti, Alexander Poddubny, Giuseppe Della Valle, Dragomir N. Neshev, Andrey A. Sukhorukov, Advanced Photonics **3**(5), 055001 (2021).
[18] Ai Du, Yi Ma, Mingfang Liu, Zhihua Zhang, Guangwei Cao, Hongwei Li, Ling Wang, Peijian Si, Jun Shen, Bin Zhou. High Power Laser Science and Engineering **9**(2), 02000e14 (2021).
[19] Tina Ebert, René Heber, Torsten Abel, Johannes Bieker, Gabriel Schaumann, Markus Roth, High Power Laser Science and Engineering **9**(2), 02000e24 (2021).
[20] J. Zhang, H. Zhang, W. Yang, K. Chen, X. Wei, Y. Feng, R. Jin, W. Zhu, Advanced Optical Materials **8**, 2000683 (2020).
[21] X. Bai, F. Kong, Y. Sun, F. Wang, J. Qian, X. Li, A. Cao, C. He, X. Liang, R. Jin, W. Zhu, Advanced Optical Materials **8**, 2000570 (2020).
[22] X. Jing, X. Gui, P. Zhou, Z. Hong, Journal of Lightwave Technology **36**(12), 2322 (2018).
[23] R. Xia, X. Jing, X. Gui, Y. Tian, Opt. Mater. Express **7**(3), 977 (2017).
[24] M. R. Akram, M. Q. Mehmood, X. Bai, R. Jin, M. Premaratne, W. Zhu, Advanced Optical Materials **7**, 1801628 (2019).
[25] M. R. Akram, X. Bai, R. Jin, G. A. E. Vandenbosch, M. Premaratne, W. Zhu, IEEE Transactions on Antennas and Propagation **67**(7), 4650 (2019).
[26] J. Zhao, X. Jing, W. Wang, Y. Tian, D. Zhu, G. Shi, Optics & Laser Technology **95**, 56 (2017).
[27] Y. Tian, X. Jing, H. Gan, X. Li, Z. Hong, Front. Phys. **15**, 62502 (2020).
[28] Y. Fu, Y. Fei, D. Dong, Y. Liu, Front. Phys. **14**, 62601 (2019).
[29] Y. Fu, Jia Tao, A. Song, Y. Liu, Y. Xu, Front. Phys. **15**, 52502 (2020).
[30] Z. Shen, H. Yang, X. Liu, X. Huang, T. Xiang, J. Wu, W. Chen, Front. Phys. **15**, 12601 (2020).
[31] J. Li, R. Jin, J. Geng, X. Liang, K. Wang, M. Premaratne, W. Zhu, IEEE Transactions on Antennas and Propagation, **67**(4), 2442 (2019).
[32] X. Lu, X. Zeng, H. Lv, Y. Han, Z. Mou, C. Liu, S. Wang, S. Teng, Nanotechnology **31**, 135201 (2020).
[33] H. Lv, X. Lu, Y. Han, Z. Mou, C. Zhou, S. Wang, S. Teng, New J. Phys. **21**, 123047 (2019).
[34] H. Lv, X. Lu, Y. Han, Z. Mou, S. Teng, Optics Letters

44(10), 2518 (2019).
[35] H. Wang, L. Liu, C. Zhou, J. Xu, M. Zhang, S. Teng, Y. Cai, Nanophotonics **8**(2), 317 (2019).
[36] X. Jing, S. Jin, Y. Tian, P. Liang, Q. Dong, L. Wang, Optics & Laser Technology **48**, 160 (2013).
[37] X. Jing, Y. Xu, H. Gan, Y. He, Z. Hong, IEEE Access **7**, 144945 (2019).
[38] L. Jiang, B. Fang, Z. Yan, J. Fan, C. Qi, J. Liu, Y. He, C. Li, X. Jing, H. Gan, Z. Hong, Optics & Laser Technology **123**, 105949 (2020).
[39] S. Liu, L. Zhang, Q. Yang, Q. Xu, Y. Yang, A. Noor, Q. Zhang, S. Lqbal, X. Wan, Z. Tian, W. Tang, Q. Cheng, J. Han, W. Zhang, T. Cui, Adv. Opt. Mater. **4**(12), 1965 (2016).
[40] T. Cui, M. Qi, X. Wan, J. Zhao, Q. Cheng, Light-Science & Applications **3**(10), e218 (2014).
[41] Z. Ma, S. Hanham, P. Albella, B. Ng, H. Lu, Y. Gong, S. Maier, M. Hong, ACS Photon. **3**(6), 1010 (2016).
[42] L. W. Zhu, Y. Y. Cao, Q. Q. Chen, X. Ouyang, Y. Xu, Opto.-Electron. Adv. **4**, 210002 (2021).

*Corresponding author: 154495791@qq.com